mathematics

MDPI

Article

Feature Detection Based on Imaging and Genetic Data Using Multi-Kernel Support Vector Machine–Apriori Model

Zhixi Hu [1], Congye Tang [1], Yingxia Liang [1], Senhao Chang [1], Xinyue Ni [1], Shasha Xiao [1], Xianglian Meng [1], Bing He [2,*] and Wenjie Liu [1,*]

[1] School of Computer Science and Information Engineering, Changzhou Institute of Technology, Changzhou 213002, China; huzx@czust.edu.cn (Z.H.); 20030522@czust.edu.cn (C.T.); 21030612@czust.edu.cn (Y.L.); 20030905@czust.edu.cn (S.C.); 22030416@czust.edu.cn (X.N.); xiaoss@czust.edu.cn (S.X.); mengxl@czust.edu.cn (X.M.)

[2] Luddy School of Informatics, Computing and Engineering, Indiana University-Purdue University Indianapolis, Indianapolis, IN 46202, USA

* Correspondence: hebing@iu.edu (B.H.); liuwj@czust.edu.cn (W.L.)

Abstract: Alzheimer's disease (AD) is a significant neurological disorder characterized by progressive cognitive decline and memory loss. One essential task is understanding the molecular mechanisms underlying brain disorders of AD. Detecting biomarkers that contribute significantly to the classification of AD is an effective means to accomplish this essential task. However, most machine learning methods used to detect AD biomarkers require lengthy training and are unable to rapidly and effectively detect AD biomarkers. To detect biomarkers for AD accurately and efficiently, we proposed a novel approach using the Multi-Kernel Support Vector Machine (SVM) with Apriori algorithm to mine strongly associated feature sets from functional magnetic resonance imaging (fMRI) and gene expression profiles. Firstly, we downloaded the imaging data and genetic data of 121 participants from the Alzheimer's Disease Neuroimaging Initiative (ADNI) and transformed gene sequences into labeled sequences by encoding the four types of bases (A, T, C, and G) into distinct labels. Subsequently, we extracted the first 130 temporal sequences of brain regions and employed Pearson correlation analysis to construct "brain region gene pairs". The integration of these data allowed us to explore the correlations between genes and brain regions. To improve classification accuracy and feature selection, we applied the Apriori algorithm to the multi-kernel SVM, dynamically building feature combinations and continuously validating classification results. By iteratively generating frequent itemsets, we obtained important brain region gene pairs. Experimental results show the effectiveness of our proposed approach. The Multi-Kernel SVM with Apriori model achieves an accuracy of 92.9%, precision of 95%, and an F1 score of 95% in classifying brain region-gene pairs within the AD–Late mild cognitive impairment (AD-LMCI) group. The amygdala, *BIN1*, *RPN2*, and *IL15* associated with AD have been identified and demonstrate potential in identifying potential pathogenic factors of AD. The selected brain regions and associated genes may serve as valuable biomarkers for early AD diagnosis and better understanding of the disease's molecular mechanisms. The integration of fMRI and gene data using the Multi-Kernel SVM–Apriori model holds great potential for advancing our knowledge of brain function and the genetic basis of neurological disorders. This approach provides a valuable tool for neuroscientists and researchers in the field of genomics and brain imaging studies.

Keywords: Alzheimer's disease; SVM; Apriori algorithm; brain region-gene pairs; frequent itemset

MSC: 68W20; 68W40

Citation: Hu, Z.; Tang, C.; Liang, Y.; Chang, S.; Ni, X.; Xiao, S.; Meng, X.; He, B.; Liu, W. Feature Detection Based on Imaging and Genetic Data Using Multi-Kernel Support Vector Machine–Apriori Model. *Mathematics* **2024**, *12*, 684. https://doi.org/10.3390/math12050684

Academic Editor: Vince Grolmusz

Received: 12 January 2024
Revised: 22 February 2024
Accepted: 24 February 2024
Published: 26 February 2024

1. Introduction

1.1. Background

Alzheimer's disease (AD) is a progressive neurodegenerative disorder that is characterized by a decline in cognitive abilities and memory loss [1,2]. It affects millions of people worldwide, and the number of cases is expected to increase as the population ages. Early detection and accurate diagnosis of AD are crucial for effective treatment and management of the disease. Considering that changes in synaptic function occur early in neurodegenerative processes, functional magnetic resonance imaging (fMRI) is particularly promising for detecting early changes in brain function [3,4]. In the early diagnosis of AD, the detection of biomarkers is crucial. The current topic lies in effectively identifying biomarkers that contribute significantly to AD classification.

One approach to diagnosing AD is through the analysis of brain imaging data, such as magnetic resonance imaging (MRI) and positron emission tomography (PET). The use of machine learning algorithms, such as support vector machine (SVM), has shown promise in accurately classifying patients with AD from healthy controls based on these imaging data.

The aim of using Apriori algorithms and support vector machine (SVM) in Alzheimer's disease (AD) research is to improve the accuracy of AD diagnosis and classification using brain imaging data.

Apriori algorithms incorporate Apriori probabilities about the disease into the machine learning algorithm to improve its performance. This Apriori knowledge can include information about the brain regions affected by AD or the probability of a patient having the disease based on demographic and clinical factors.

SVM is a machine learning algorithm that can be used to classify patients with AD from healthy controls based on brain imaging data. SVM works by finding a hyperplane that separates the data points into different classes, with the goal of maximizing the margin between the hyperplane and the closest data points. SVM can also be used to handle high-dimensional data, such as brain imaging data, which can be useful in AD research where there are many variables to consider.

1.2. Related Work

Apriori algorithms and support vector machine (SVM) have various applications in different fields. Below are some typical applications of these algorithms.

Huang et al. [5] analyzed the prevalence of multiple chronic diseases using 8477 participants aged >45 years from the "2020 Korean Health Panel Survey" and found that cardiovascular diseases (150%), spondylosis (143%), and diabetes (125%) were the three chronic diseases with the highest frequency increases. Vougas et al. [6] described a novel computer screening process based on association rule mining, used to identify genes as candidate driving factors for drug response. Liu et al. [7] proposed an association rule data mining algorithm that combines clustering matrices and pruning strategies, reducing the number of database scans and generating an appropriate number of candidate itemsets, significantly reducing runtime. Hadavi et al. [8] utilized medical records spanning 5 years from 512 esophageal cancer patients and those with related issues to create six significant association rules. Ultimately, they discovered significant associations among age, medical history, smoking, gender, carcinoembryonic antigen, creatinine, white blood cells, and platelets.

The SVM [9–11] has been widely used in AD classification due to its ease of use and understanding. Lai et al. [12] proposed a method using nine machine learning algorithms, including SVM and K Nearest Neighbor (KNN), to select Entity-relationship (ER)-related feature genes and estimate their efficiency in early diagnosis of AD. The SVM model achieved an Area Under Curve (AUC) of 0.879, accuracy of 0.808, recall of 0.773, and precision of 0.809. Six genes (*RNF5*, *UBAC2*, *DNAJC10*, *RNF103*, *DDX3X*, and *NGLY1*) were identified through this study. Yu et al. [13] proposed a method using LASSO and Support Vector Machine Recursive Feature Elimination (SVM-RFE) analysis to screen potential diagnostic feature genes in AD. They further tested the results in the AD brains of a validation cohort. Through this method, they identified a total of 49 differentially

expressed genes (*DEGs*). Among them, *MAFF*, *ADCYAP1*, and *ZFP36L1* were determined as diagnostic biomarkers for AD, with an AUC of 0.850 in the model, and further validated in the validation cohort with an AUC of 0.935. Yang et al. [14] proposed a method based on the forgeNet_SVM model for feature extraction from three molecular fusion feature sets (*ECFP6*, *MACCS*, and *RDKit*). The results showed that the feature set selected by SVM outperformed the fusion-feature set and single-feature sets. SVM demonstrated higher accuracy in identifying compounds related to Alzheimer's disease. Zhang et al. [15] proposed an algorithm model that combines Support Vector Machine Recursive Feature Elimination and Leave-One-Out Cross-Validation (SVM-RFE-LOO) for early detection of AD. The results showed that this model reduced the number of features from 21 to 16, with an AUC of 0.980, sensitivity of 94.0%, and specificity of 93.3%. After applying a forward feature selection technique, Olatunji et al. [16] used SVM to construct a model for screening AD, achieving an accuracy of 95.56%, precision of 94.70%, and recall of 97.78%.

The combination of multimodal data for feature selection has been widely used in mild cognitive impairment (MCI) and AD classification studies. Traditional multimodal feature selection methods have limitations, as they do not consider the correlation between feature points and local feature space. To address this issue, Jiao et al. [17] proposed a multimodal feature selection algorithm called Feature and Concept Fusion (FC2FS), which fused the final features and inputted them into SVM for classification. The experimental results showed that SVM has advantages in MCI and AD classification. In the SVM model, the accuracy for AD-healthy control (HC), Late MCI-HC, Early MCI-HC, and EMCI-LMCI were 91.85 $\pm$ 1.42%, 85.33 $\pm$ 2.22%, 78.29 $\pm$ 2.20%, and 77.67 $\pm$ 1.65%, respectively. Syaifullah et al. [18] developed a software called Brain Anatomical Analysis Using Diffeomorphic Deformation (BAAD, BAAD HP en (shiga-med.ac.jp)), which can diagnose AD and MCI patients using machine learning algorithms. They achieved an accuracy of 90.5% by combining SVM for classification and the voxel-based morphometry (VBM) technique to reduce correlated variables. Houria et al. [19] proposed a method that combines multi-modal MRI to detect changes in white matter (WM) and gray matter (GM). They fused features extracted from diffusion tensor imaging (DTI) and features extracted from GM using a two-dimensional (2D) convolutional network. These features were then input into SVM for classification in each stage. The final accuracy for AD/HC, AD/MCI, and MCI/HC classification reached 99.79%, 99.6%, and 97.00%, respectively.

However, while Apriori algorithms and support vector machine (SVM) have shown promising results in Alzheimer's disease (AD) research, there are also some disadvantages in using these algorithms. The performance of Apriori algorithms is highly dependent on the accuracy and relevance of the Apriori knowledge used. If the Apriori knowledge is inaccurate or incomplete, it can negatively impact the accuracy of the AD diagnosis. It can be difficult to quantify Apriori knowledge in a meaningful way, which can make it challenging to incorporate it into the machine learning algorithm. This can lead to subjective decisions and biases in the algorithm. While SVM can accurately classify patients with AD from healthy controls, the decision process of SVM relies more on mathematical decisions than pathological processes. Therefore, how to match pathological processes with mathematical decisions is a problem that needs to be addressed. This lack of interpretability can make it challenging to understand the underlying mechanisms of the disease.

However, one of the challenges in using machine learning algorithms for AD diagnosis is the limited availability of labeled data, which can hinder the performance of the models. In this regard, Apriori knowledge or information can be incorporated into the algorithms to improve their performance. The use of Apriori algorithms has been shown to improve the classification accuracy of machine learning algorithms in medical imaging data analysis [6].

1.3. Proposed Framework

In this paper, we explored the use of Apriori algorithms in SVM for the classification of AD patients and healthy controls based on brain fMRI data. We investigated the performance of the SVM algorithm with the incorporation of Apriori algorithms in the form of

frequent items. We also compared the performance of our proposed approach with other SVM models for AD diagnosis. The overall description of the model is shown in Figure 1.

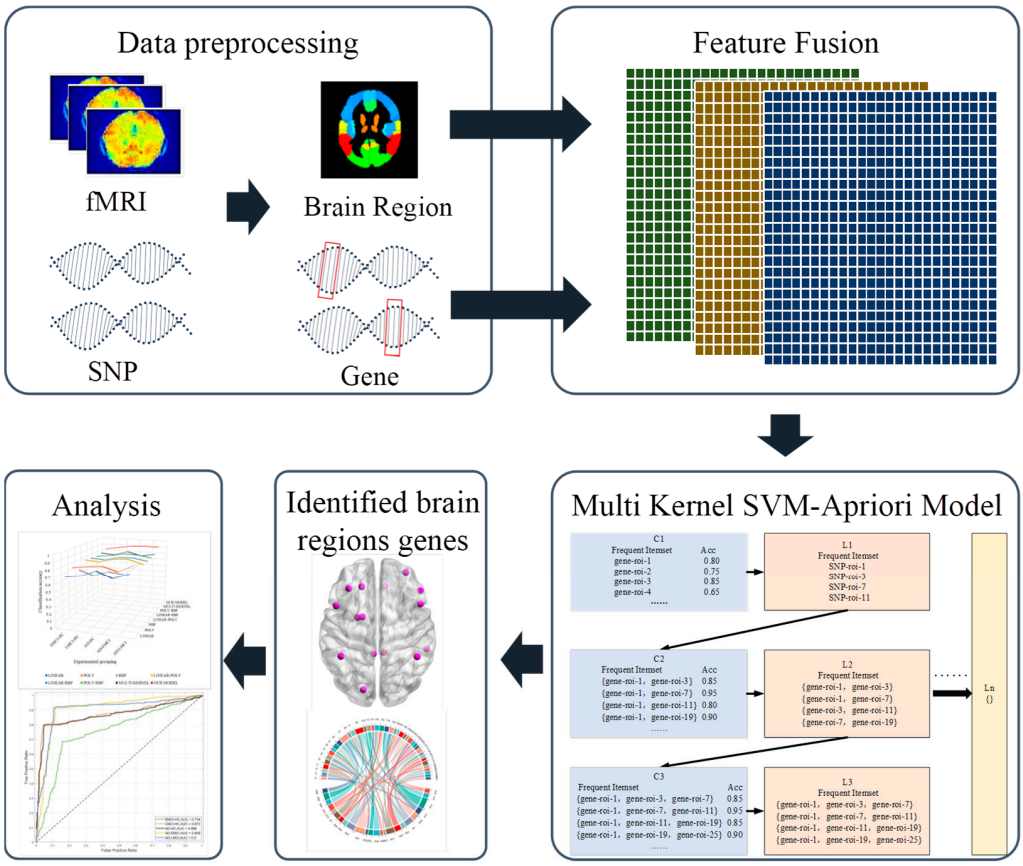

Figure 1. The framework of Multi Kernel SVM–Apriori Model analysis.

Specifically, we combined the fMRI data and gene data to discriminate between AD and healthy control (HC), or between AD and early MCI, or between AD and late MCI, or between late MCI and HC, or between early MCI and HC. To effectively combine the different data for classification, we used a simple but effective data fusion method and proposed an approach based on Apriori algorithms. This approach introduced frequent itemsets from Apriori algorithms, which could be naturally embedded into traditional SVM classifiers, thereby enhancing the classification performance and finding the significant biomarkers. Our findings suggest that the incorporation of Apriori algorithms could significantly improve the performance of the SVM algorithm for AD diagnosis and could potentially aid in the early detection and management of the disease.

2. Materials and Methods

2.1. Data Pre-Processing

Data used in our study were downloaded from the ADNI database (adni.loni.usc.cn). The fMRI imaging of 121 participants, including 53 males and 68 females, were obtained. The details of these participants are shown in Table 1.

We calculated the mean and standard deviation of age and years of education and computed the correlation between gender, age, years of education, and diagnostic status. The results indicate a significant correlation.

Table 1. The participants' characteristics. HC = Healthy Control; EMCI = Early Mild Cognitive Impairment; LMCI = Late Mild Cognitive Impairment; AD = Alzheimer's Disease; P = *p*-value; EDU = Education.

Subjects	HC	EMCI	LMCI	AD	P
Number	42	31	24	24	-
Gender (M/F)	19/23	12/19	14/10	8/16	<0.001
Age (Mean ± sd)	74.2 ± 6.1	72.8 ± 6.4	70.9 ± 8.3	72.0 ± 7.6	<0.001
EDU (Mean ± sd)	16.5 ± 2.7	15.8 ± 2.7	16.8 ± 2.6	15.5 ± 2.9	<0.001

All neuroimaging data were obtained using a SIEMENS 3T MRI scanner. We used the DPARSF [20] tool to set image parameters such as timepoints, TR (repetition time), and reference slice image to 140, 3, and 47, respectively. During the MRI scans, the stability of the gradient magnetic field and participant adaptation required some time. As a result, the initial few timepoints of the images tended to have more noise. To ensure the stability of the magnetic field gradient in the scanner, the first 10 timepoints of all participants were removed.

The preprocessing of fMRI images is shown in Figure 2. The participants' T1 and fMRI images were preprocessed by skull stripping, head motion correction, and normalization. To reduce registration inaccuracies and improve signal-to-noise ratio, we utilized a smoothing process with a Gaussian kernel size of 4 mm full width at half maximum (FWHM) and a frequency range of 0.01 Hz to 0.08 Hz to remove noise from the images. Finally, the Automated Anatomical Labeling (AAL) atlas116 template was used to define brain regions and extract time series data from these regions [21,22].

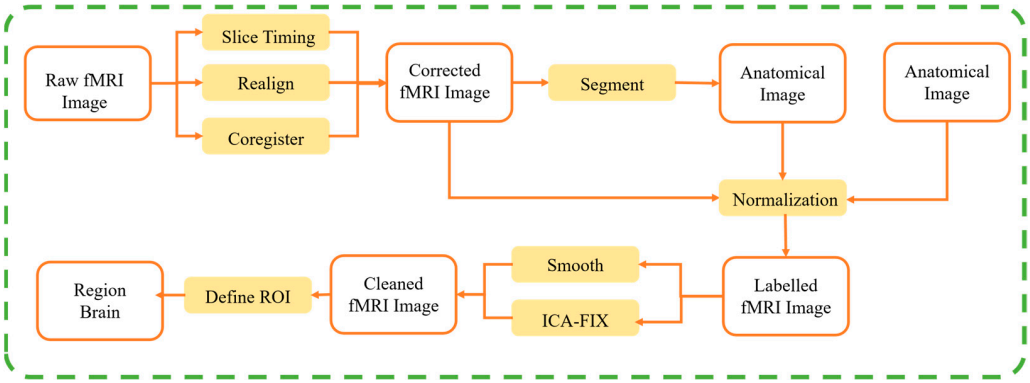

Figure 2. The preprocessing flowchart of fMRI. fMRI data preprocessing pipeline includes: Data Format Conversion (from DICOM to Neuroimaging Informatics Technology Initiative), Removal of Unstable Time Points, Slice Timing Correction, Head Motion Correction, Spatial Normalization, Spatial Smoothing, Detrending, Filtering, and Registration.

The Illumina Genome-wide Association Study (GWAS) arrays (610-Quad, OmniExpress or HumanOmni2.5-4v1) (Illumina, Inc., San Diego, CA, USA) and blood genomic DNA samples were used to genotype the participants [23]. Then, we applied PLINK v1.9 [24] to extract single nucleotide polymorphisms (SNPs) using the following process: (1) extracting SNPs on chromosome 1–22; (2) call rate of each SNP $\geq$ 95%; (3) minor allele frequency of each SNP $\geq$ 5%; (4) Hardy–Weinberg equilibrium test $p \geq 1.0 \times 10^{-6}$; (5) call rate of each participant $\geq$ 95%. Finally, we extracted the genes with SNP number $\geq$ 130 and obtained 280 gens and 36,400 SNPs.

2.2. Features Fusion

In order to build fused features and detect correlations between genes and brain regions, we converted the four types of bases within genes (such as A, T, C, and G) into different labels (e.g., AT = 0, CG = 0, AC = 1, AG = 2, TC = 3, TG = 4) to obtain a labeled

sequence for the genes. The first 130 temporal sequences of the brain regions were extracted, and Pearson correlation analysis was employed to construct brain region gene pairs.

For the gene data, we selected genes with more than 130 SNPs within them and obtained 280 genes. Then, we extracted the first 130 data points of each gene sequence. As a result, we filtered out 280 genes and saved them as a matrix M_{gene}, as shown in Formula (1).

$$M_{gene} = \{bp_{ij}\}, \ i \in [1, 280], \ j \in [1, 130] \tag{1}$$

where i represents the gene number and j represents the SNP position. The gene dataset size is 280×130.

A similar process was applied to brain regions (removing the first 10 timepoints). For the fMRI data, we calculated the brain region signals for each participant across 130 time series using 90 brain regions from the AAL atlas. These signals were then saved as a matrix M_{roi}, as shown in Formula (2).

$$M_{roi} = \left\{ROI_{jk}\right\}, \ j \in [1, 130], \ k \in [1, 90] \tag{2}$$

where j represents the time series of brain region and k represents the brain region. There are a total of 121 samples, and the brain region signal dataset size is $121 \times 130 \times 90$.

Then, we used Pearson correlation [25] analysis to integrate the brain region data and gene data. The formula for Pearson correlation analysis was defined as Formula (3), and the obtained matrix was shown as Formula (4).

$$\rho_{M_{gene},\, M_{roi}} = \frac{E\left(M_{gene}[i,:] \cdot M_{roi}[:,k]\right) - E\left(M_{gene}[i,:]\right) \cdot E(M_{roi}[:,k])}{\sqrt{E\left(M_{gene}[i,:]^2\right) - E^2\left(M_{gene}[i,:]\right)}\sqrt{E\left(M_{roi}[:,k]^2\right) - E^2(M_{roi}[:,k])}}, \tag{3}$$

where $\rho_{M_{gene},\, M_{roi}}$ is the feature matrix that fused brain region and gene data. $E\left(M_{gene}[i,:]\right)$ is the mean of $M_{gene}[i,:]$. $E(M_{roi}[:,k])$ is the mean of $M_{roi}[:,k]$. $E\left(M_{gene}[i,:] \cdot M_{roi}[:,k]\right)$ is the mean of the product of $M_{gene}[i,:]$ and $M_{roi}[:,k]$. $E\left(M_{gene}[i,:]^2\right)$ and $E\left(M_{roi}[:,k]^2\right)$ are the means of the squares of each element in $M_{gene}[i,:]$ and $M_{roi}[:,k]$. $E^2\left(M_{gene}[i,:]\right)$ and $E^2(M_{roi}[:,k])$ are the squares of the mean of elements in $M_{gene}[i,:]$ and $M_{roi}[:,k]$.

$$M_{gene-roi} = \{Gene_i \cdot Roi_k\}, \qquad i \in [1, 280], \ k \in [1, 90] \tag{4}$$

where Gene_i represents the ith row vector Gene_i of M_{gene} and Roi_k represents the kth column vector Roi_k of M_{roi}. $\text{Gene}_i \cdot Roi_k$ denotes the matrix product between the row vector $Gene_i$ from M_{gene} and column vector Roi_k from M_{roi}.

2.3. Multi-Kernel SVM-Apriori Model Construction

The Apriori algorithm was applied to the multi-kernel SVM, utilizing the strengths of both algorithms.

The Multi-Kernel SVM–Apriori Model was constructed as Algorithm 1.

This involved dynamically constructing feature combinations, continuously validating the classification results, and sequentially verifying all data to avoid random occasional errors and ensure consistent outcomes at each step of the experiment.

Firstly, the dataset was divided into training and validation sets in a 7:3 ratio. The initial sample set was sequentially sampled to calculate its classification performance for feature selection, and the features obtained were validated using the leave-one-out method. Then, the obtained features were combined in pairs, and the combined features were checked for being frequent itemsets for further selection. This process was repeated until no new frequent itemsets could be generated.

Algorithm 1. The algorithm process of the Multi-Kernel SVM–Apriori Model

Input: experimental dataset {*X*,*Y*}; *X* is input, *Y* is the corresponding label (1 or −1) *d*, σ, ACC_{Thre}
Output: Multi-Kernel SVM–Apriori Model

1: Initialize {*X*, *Y*}, w1, w2, w3, $min_{support}$
{*X*, *Y*} is experimental dataset,
w1, w2, w3 are the weights of three kernels Equation (7),
d is the degree of a polynomial (3),
σ is the width of the Gaussian kernel (0.005),
ACC_{Thre} is the minimum support for generating frequent itemsets Equation (9).
2: Randomly select a subset of features as {Features}tra_k
3: Input {Features}tra_k according to 7:3 training, partitioning the {*X*, *Y*} into {*X*, *Y*}$_{train}$, {*X*, *Y*}$_{valid}$
4: Calculate predicted values: y_{pred} = sign (w′ × x + b)
Output: classifier: Acc = Σ (y_{pred} == *y*)/length(*y*)
5: Input set {*X*, *Y*} to Multi-kernel SVM to obtain the *Acc* of all individual features and obtain the frequent itemset L1 which satisfies $Acc > ACC_{Thre}$
6: For each k starting from k = 2:
Repeat
7: Generate candidate feature set C_k by connecting frequent itemsets L (k − 1)
– For each candidate feature set c in C_k:
– For each transaction t in dataset S:
– Check if c is a subset of t, and if so, increase the count of c
– Calculate Acc for each candidate feature set based on C_k
Update ACC_{Thre} = mean(ΣACC L(k − 1))
Filter to obtain frequent feature set Lk which satisfies $Acc > ACC_{Thre}$
Until more frequent feature sets cannot be generated, return the frequent feature set column table L
8: Finally, perform Leave-One-Out Cross-Validation for each L (k − 1) and select the feature set with the highest *ACC*.

Taking the AD-HC group as an example, there were 24 samples for AD and 42 samples for HC, making a total of 66 samples in the AD-HC group. The original dataset size was 66 × 280 × 90.

The original sample set S was defined as shown in Formula (5).

$$S = \{x_i, y_i\}, \quad i \in [1, N] \tag{5}$$

where x_i represent the features in the dataset, and the value of y_i was either 1 or −1, representing the corresponding label for x_i. HC was represented as "−1," and AD was represented as "1." N was the total number of participants.

The training and validation sets were randomly generated from the original sample set, and their corresponding proportions were set according to Formula (6).

$$S_{train} : S_{test} = 7 : 3 \tag{6}$$

where S_{train} is the training set and S_{test} is the test set.

Due to the brain region gene pairs dataset being non-linearly separable in two-dimensional space, the concept of multiple kernels was introduced. This involved mapping the samples from the original space to a higher-dimensional feature space, where the samples became linearly separable. Three kernel functions were used: the linear kernel, the polynomial kernel, and the Gaussian kernel, with weights [26] of w_1:w_2:w_3 ($w_1 \in [0.1, 1]$, $w_2 \in [0.1, 1]$, $w_3 \in [0.1, 1]$), as shown in Formula (7).

$$k = w_1 x^T x_j + w_2 (x^T x_j)^d + w_3 exp\left(-\frac{\|x_i - x_j\|}{2\gamma^2}\right) \tag{7}$$

where w_1, w_2, w_3 are the weight of the kernels. x^T is the transpose of the training set, and x_j is the test set. d is a positive integer, k is a positive real number, both using default parameters.

To obtain the original validation features using the multi-kernel SVM, the 25,200 features along with their corresponding labels were sequentially validated. The process involved using the fixed threshold of 0.80 for screening. The definition of the classification performance of the multi-kernel SVM is shown in Formula (8).

$$ACC_k = \frac{N_{vk}}{N_V} \tag{8}$$

where 'k' represents the classification performance of frequent itemsets. N_{vk} denotes the number of samples correctly classified by 'k' frequent itemsets in the validation set. N_V is the number of samples in the validation set.

Afterward, the concept of frequent itemsets was introduced, and the original features were combined in pairs. This set was defined as candidate 2 (C2).

Since the classification performance of the features filtered in the first step was superior compared to the feature set, the classification performance of the subsequent feature combinations was guaranteed to be above 0.8. Therefore, we further filtered features based on the average accuracy (ACC) of the Level 1 frequent itemset (L1) features, ensuring the elimination of features with slightly lower classification performance than those in L1. The threshold is defined as shown in Formula (9).

$$ACC_{Thre} = sum(ACC_{L1})/length(L1) \tag{9}$$

where ACC_{L1} is the accuracy of every element in frequent itemset $L1$. $length(L1)$ is the number of frequent itemset $L1$. ACC_{Thre} is the threshold used for filtering out two frequent itemsets.

After filtering, the obtained feature combinations were considered as the more significant brain region gene pairs. This set of features was referred to as two frequent itemsets and defined as L2. L2 was combined to form candidate itemsets C3 based on the principle of Apriori knowledge.

The above steps were repeated until no new frequent itemsets could be generated. Finally, we validated the classification performance of the obtained L1, L2, ..., Ln frequent itemsets using the leave-one-out validation method. The feature set with the best classification performance was considered as the most important feature set.

2.4. Model Comparison

Besides the methods described in Section 2.3, the decision tree and Apriori algorithm were used to construct the decision tree–Apriori model. The steps of the decision tree–Apriori model are shown in Figure 3.

We used the 25,200 features obtained from Section 2.3 and the decision tree to calculate the accuracy of every feature. Subsequently, we applied the fixed threshold of 0.80 to filter out the features, and the resulting features were defined as L1. The features in L1, when combined pairwise, formed the dataset C2, and the ACC of every feature pair in C2 were calculated using the decision tree. Then, the average ACC of the L1 features was introduced to select the brain region gene pairs with their corresponding ACC above the average ACC. The resulting sets were defined as 2 frequent itemsets, named L2. The above steps were repeated until no new frequent itemsets could be generated.

To demonstrate that the Apriori algorithm indeed enhanced the classification performance of the multi-kernel SVM, the single-kernel SVM, dual-kernel SVM, multi-kernel SVM, the single-kernel SVM with the Apriori algorithm and dual-kernel SVM with the Apriori algorithm were used as control groups. The Classification and Regression Tree, Random Forest, Bayes, Back Propagation Neural Network, Product-based Neural Networks, Convolutional Neural Network and Fully Connected Neural Network were also

employed to select the optimal features. To ensure the credibility of the results, we used the leave-one-out cross-validation method to obtain the results for all models.

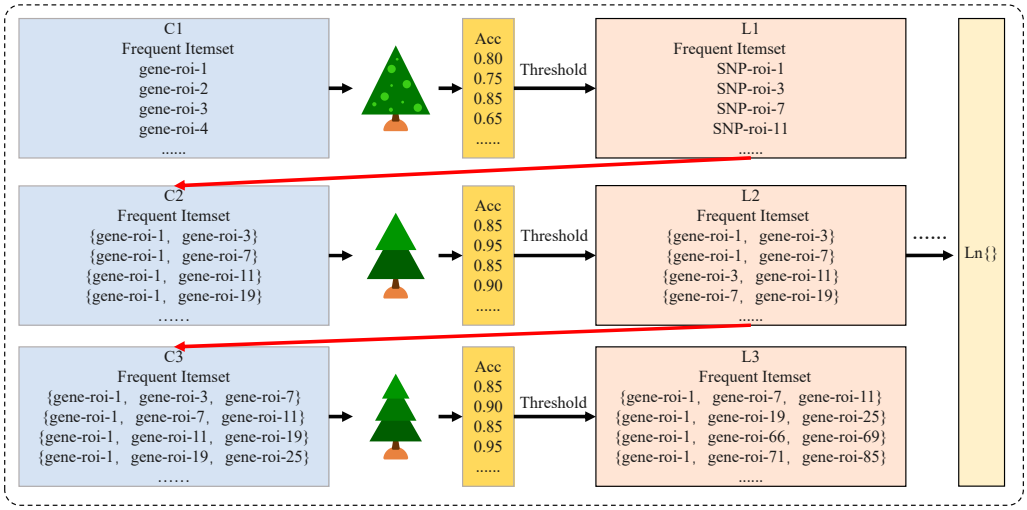

Figure 3. The steps of the decision tree–Apriori model.

3. Results

We used the S_{AD_HC} as the dataset S. Initially, we divided the dataset S into training and validation sets in a 7:3 ratio. Using a threshold of 0.8, we employed the multi-kernel SVM to filter the original 25,200 features using the resulting weight 1:1:1. The curve of weight selection is shown in Figure 4.

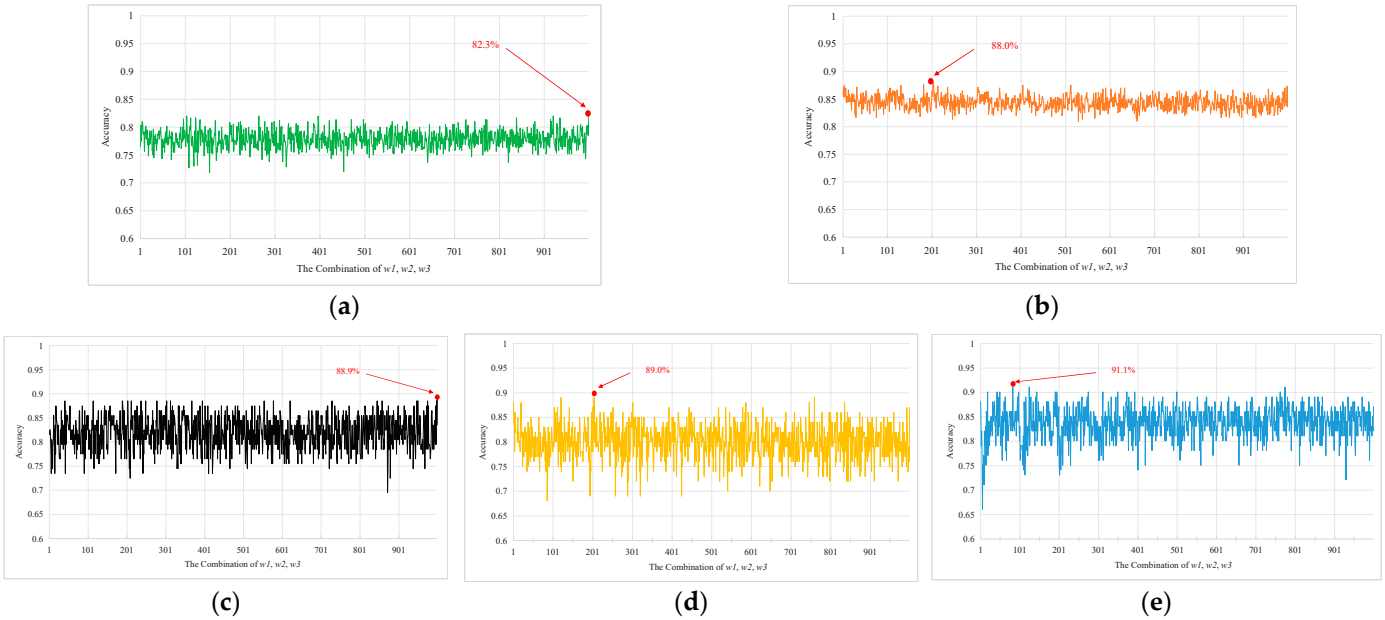

Figure 4. The combination of w_1, w_2, w_3 and their accuracy in five datasets. (**a**) The combination of w_1, w_2, w_3 and their accuracy in S_{EMCI_HC}. (**b**) The combination of w_1, w_2, w_3 and their accuracy in S_{LMCI_HC}. (**c**) The combination of w_1, w_2, w_3 and their accuracy in S_{AD_HC}. (**d**) The combination of w_1, w_2, w_3 and their accuracy in S_{AD_EMCI}. (**e**) The combination of w_1, w_2, w_3 and their accuracy in S_{AD_LMCI}.

Then, we obtained 239 features to generate the initial frequent itemset named L1. We combined these 239 features in pairs to create a new set of features, resulting in 28,441 feature combinations. Since the selected features have accuracy rates above 0.8, the accuracy of the combined features is also above 0.8. At this point, using 0.8 as the

threshold would not be able to filter out the optimal features. Therefore, we use the average accuracy of L1 as the new threshold. After the filtering process, the obtained features were used as the dataset to generate the two frequent itemsets based on the definition of frequent itemsets. We defined the two frequent itemsets as L2. The above steps were repeated until no new frequent itemsets could be generated. The difference of Ln is shown in Table 2. We tallied the features present in each frequent itemset and used these features for leave-one-out cross-validation to determine which frequent itemset's selected features were the optimal ones. To ensure the credibility of the results, we validated our model using four additional datasets. The results are shown in Figure 5.

Table 2. The association and difference between Ln. S = The initial dataset; ACC_{Ln-1} = The accuracy of every element in Ln − 1.

	L1	**L2**	**L3**	**L4**	...	**Ln**
Generate From	S	L1	L2	L3	...	Ln−1
Accuracy Threshold	0.8	mean(ACC_{L1})	mean(ACC_{L2})	mean(ACC_{L3})	...	mean(ACC_{Ln-1})

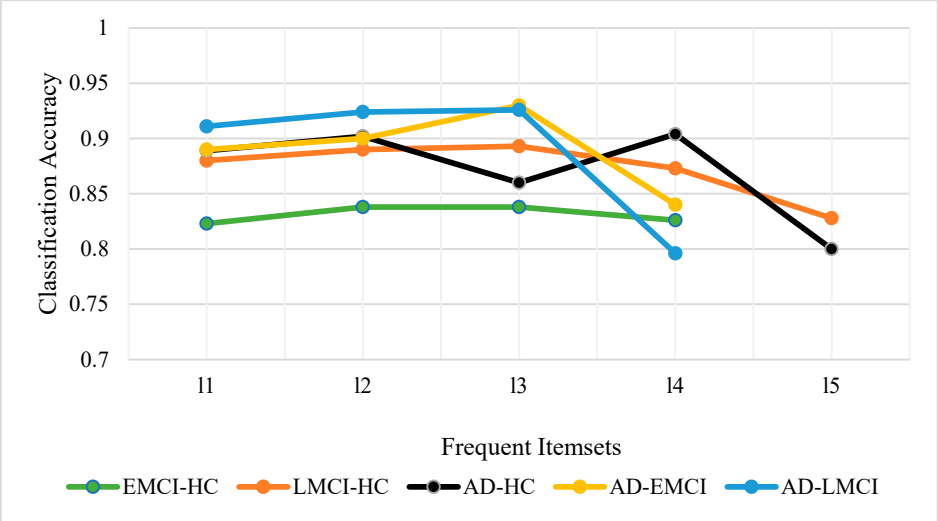

Figure 5. The accuracy of leave-one-out cross-validation of the test set of all frequent itemsets in 5 datasets.

The L1 is generated from the initial dataset, and the accuracy threshold is 0.8. The generation of L2 to Ln relies on the previous frequent itemset, and the accuracy threshold is the average of the accuracy of the previous frequent itemset.

We observe fluctuating changes in the accuracy shown in Figure 5. The leave-one-out cross-validation accuracy of L1 is 88.9%, while the accuracy of L2 improves to 90.2%. However, the accuracy of L3 decreases to 86%, and the accuracy of L4 increases again to 90.4%. L5 has the lowest accuracy, declining to 80%. This indicates that the initial screening of L1 retained most of the outstanding features. After L2 filtering, some features with poor classification performance were eliminated, leading to an accuracy improvement. The decrease in accuracy for L3 may be due to the retention of features with lower classification performance during the generation of L3 while eliminating features with better classification performance, which is also the case for L5. The increase in accuracy for L4 suggests that during the generation of L4, some features with poor classification performance were eliminated once again. We also observe that the highest accuracy was achieved in the AD-EMCI group with L4, reaching 91.45%. Following that, the AD-LMCI group with L2 and the AD-HC group with L4 achieve accuracies of 91.2% and 90.4%, respectively. In the five sets of data, as the number of features decreases, good features are selected while poor features are discarded. This may be the reason for the increase in accuracy

and is the purpose of integrating the prior algorithm. The accuracies for the EMCI-HC and LMCI-HC groups are slightly lower, at 87.2% and 83.8%, respectively. This could be due to the smaller differences between the EMCI group and HC group, resulting in lower accuracy. On the other hand, the larger differences between the data in other groups led to better classification performance. Considering the conditions of five datasets, the proposed method can obtain the optimal feature set after filtering in one of the frequent itemsets.

We also employed the single-kernel SVM, dual-kernel SVM and the multi-kernel SVM to select the optimal features. The curve of weight selection of dual-kernel SVM in S_{AD_HC} is shown in Figure 6. The comparison results using leave-one-out cross-validation with our model are shown in Figure 7. The F1 score, recall and precision are presented in Table 3.

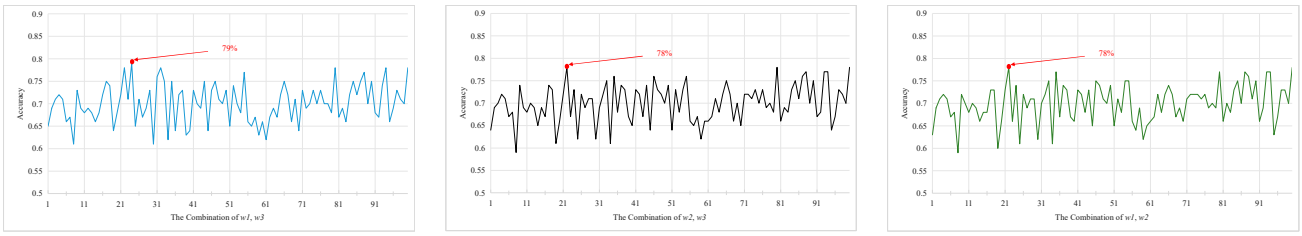

(**a**) (**b**) (**c**)

Figure 6. The curve of weight selection of dual-kernel SVM in S_{AD_HC}. (**a**) The combination of w_1, w_3 and their accuracy in S_{AD_HC}. (**b**) The combination of w_2, w_3 and their accuracy in S_{AD_HC}. (**c**) The combination of w_1, w_2 and their accuracy in S_{AD_HC}.

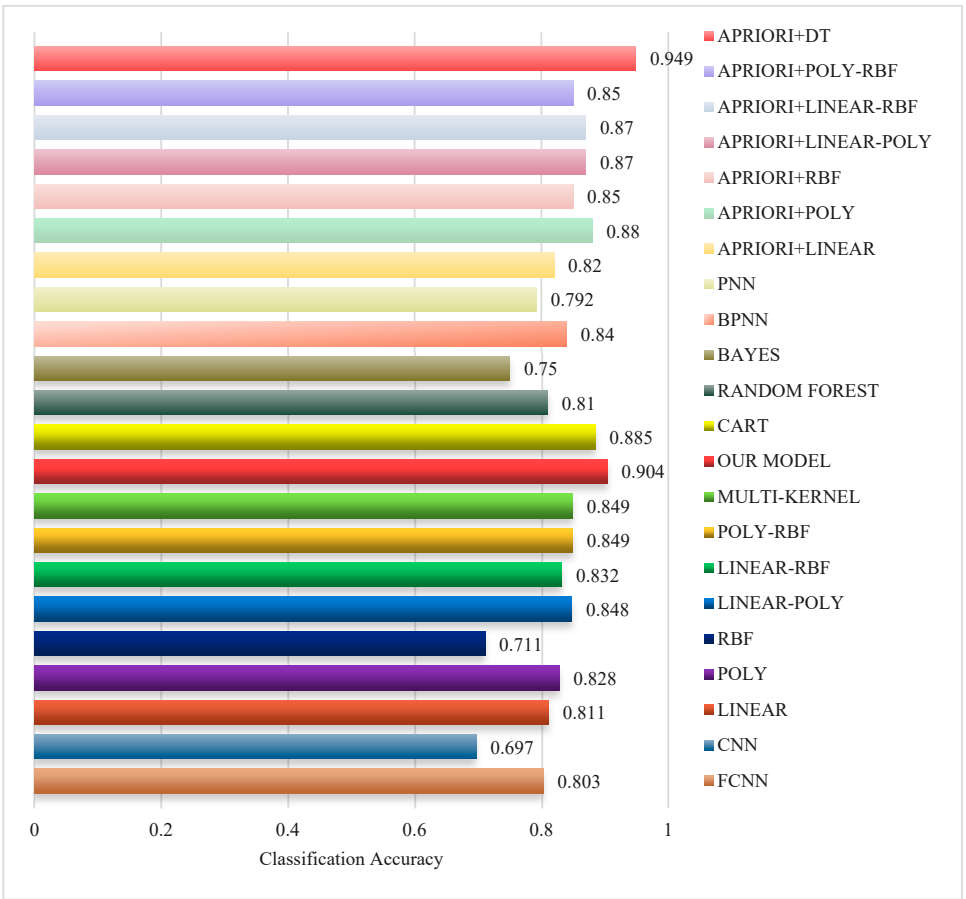

Figure 7. The comparison with other methods in S_{AD_HC}. DT = Decision Tree; PNN = Product-based Neural Network; BPNN = Back-Propagation Neural Network; CART = Classification and Regression Tree; CNN = Convolutional Neural Network; FCNN = Fully Connected Neural Network.

Table 3. The F1 score, recall and precision of the 10 independent validation experiments in test set of S_{AD_HC}. The bold format is the model proposed in this study. DT = Decision Tree; PNN = Product-based Neural Network; BPNN = Back-Propagation Neural Network; CART = Classification and Regression Tree; CNN = Convolutional Neural Network; FCNN = Fully Connected Neural Network.

Model	Accuracy	F1 Score	Recall	Precision
LINEAR	76.25% ± 2.64%	74.8% ± 4.64%	79% ± 6.46%	71.8% ± 6.94%
POLY	76.88% ± 3.02%	74.8% ± 3.91%	79.6% ± 5.52%	71.6% ± 7.52%
RBF	78.13% ± 3.29%	77.6% ± 4.4%	81.8% ± 6.43%	74.8% ± 6.96%
LINEAR-POLY	76.25% ± 2.64%	75.6% ± 4.45%	81.9% ± 6.82%	71% ± 6.8%
LINEAR-RBF	76.88% ± 3.02%	74.9% ± 4.15%	77.3% ± 5.76%	73% ± 4.03%
POLY-RBF	76.88% ± 3.02%	76.5% ± 3.37%	76.8% ± 4.61%	76.4% ± 3.75%
MULTI-KERNEL	76.88% ± 4.22%	76.5% ± 4.53%	79.9% ± 6.12%	74.2% ± 5.07%
OUR MODEL	**90.20% ± 1.54%**	**93.20% ± 1.08%**	**93.30% ± 1.19%**	**93.50% ± 1.02%**
CART	84.44% ± 2.34%	82.2% ± 3.46%	82% ± 5.03%	83% ± 5.08%
RANDOM FOREST	84.44% ± 2.34%	81.8% ± 3.79%	83.3% ± 4.45%	80.8% ± 4.92%
BAYES	85% ± 2.68%	84.9% ± 2.92%	85.2% ± 2.82%	84.9% ± 3.07%
BPNN	72.94% ± 4.11%	76.5% ± 3.72%	82.2% ± 3.71%	71.4% ± 4.2%
PNN	82.94% ± 1.86%	84.1% ± 1.91%	86.6% ± 2.27%	81.8% ± 1.87%
APRIORI+LINEAR	86.6% ± 3.47%	90.6% ± 2.41%	91.5% ± 2.17%	90.4% ± 2.46%
APRIORI+POLY	83.4% ± 3.69%	88.7% ± 2.45%	88.9% ± 2.64%	89% ± 2.49%
APRIORI+RBF	87.8% ± 3.19%	91.3% ± 2.16%	92.1% ± 2.08%	91.3% ± 2.16%
APRIORI+LINEAR-POLY	82.1% ± 4.79%	85.5% ± 4.33%	85.5% ± 4.14%	85.7% ± 4.3%
APRIORI+LINEAR-RBF	88.6% ± 2.84%	89.1% ± 2.56%	89.9% ± 2.51%	88.9% ± 2.81%
APRIORI+POLY-RBF	82% ± 3.74%	87.7% ± 2.71%	88.2% ± 2.57%	87.6% ± 2.59%
APRIORI+DT	**94.57% ± 0.78%**	**95.6% ± 0.52%**	**95.6% ± 0.52%**	**96.5% ± 0.53%**
CNN(Overfitting)	68.03% ± 1.33%	26% ± 0%	18% ± 0%	50% ± 0%
FCNN(Overfitting)	73.09% ± 1.15%	31% ± 0%	22% ± 0%	50% ± 0%

We observe that our model had the highest accuracy, and the accuracy of the dual-kernel SVM is generally higher than that of the single-kernel SVM. This suggests that under the leave-one-out cross-validation method, the features selected by the traditional SVM did not perform well in classification. In contrast, the features selected by our model exhibited significantly better classification performance than the traditional SVM.

The receiver operating characteristic (ROC) curve of the best accuracy in each dataset is shown in Figure 8. The lowest AUC value is 0.754 in EMCI-HC dataset. The AUC values of other datasets are all above 0.86, while the best AUC value is 0.906 in AD-EMCI dataset. The model utilized on the AD-LMCI dataset exhibits the strongest capability in distinguishing between AD and LMCI. However, due to the minimal differences between EMCI and HC, its performance is poorer on the EMCI-HC dataset, consistent with the accuracy results.

Similarly, we also conducted comparisons in these datasets, and the results are presented in Figure 9.

We can observe that in all five datasets, the SVM model integrated with the Apriori algorithm and the decision tree model integrated with the Apriori algorithm performed the best, achieving the highest accuracy, of 91.45% and 94.9%. The dual-kernel SVM integrated with the Apriori algorithm achieved an accuracy of 88%. Additionally, its stability across five datasets was higher than that of the traditional SVM. In contrast, the highest accuracy achieved by the traditional SVM was 87.5%. This indicates that the introduction of the Apriori algorithm enables SVM to achieve higher accuracy and select more important features. However, due to the limited sample size of only 121, and the fusion of imaging and genetic data, there are insufficient data. Consequently, overfitting occurred during the training of the deep learning models.

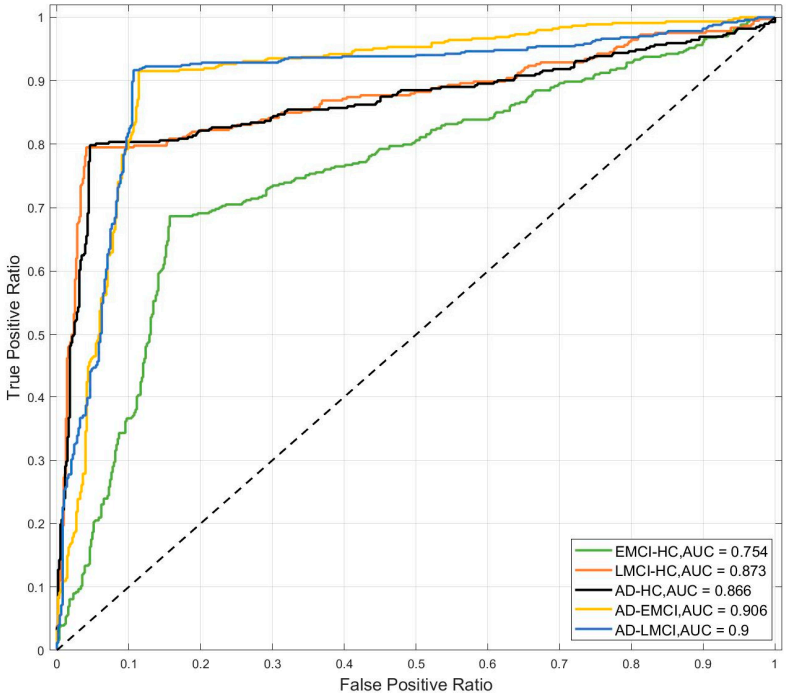

Figure 8. The ROC curve of the best accuracy in each dataset. The dashed line represents the performance of a random classifier.

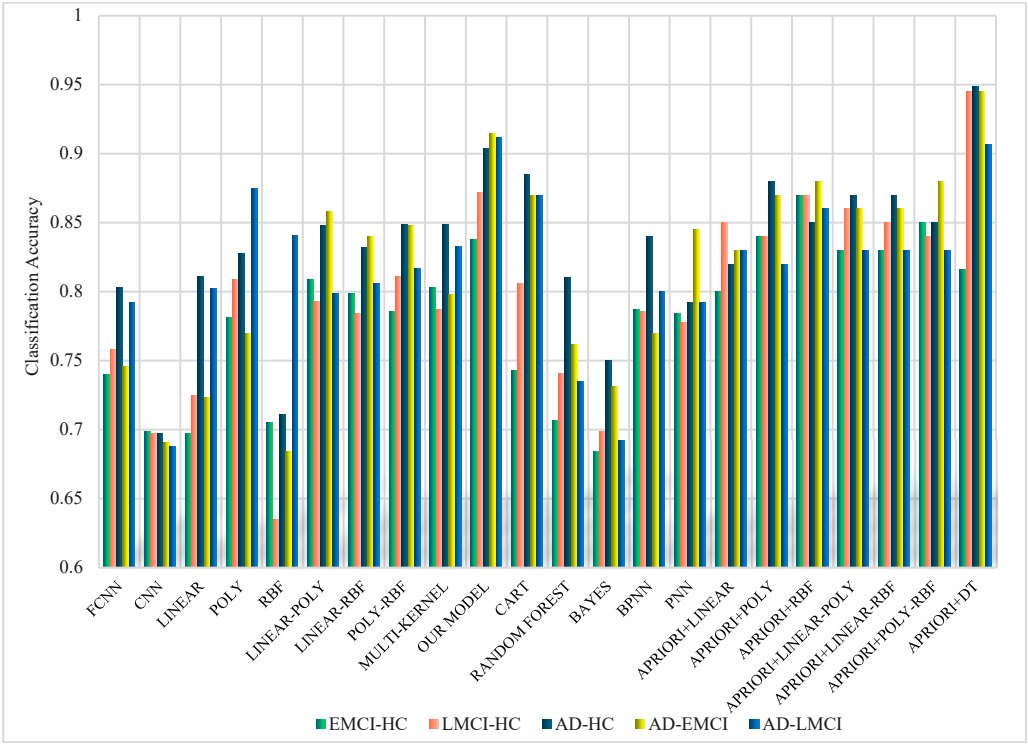

Figure 9. The comparison with other methods in 5 datasets. DT = Decision Tree; PNN = Product-based Neural Network; BPNN = Back-Propagation Neural Network; CART = Classification and Regression Tree; CNN = Convolutional Neural Network; FCNN = Fully Connected Neural Network.

To verify the stability of our model, we conducted 10 independent validation experiments on five datasets. The results are presented in Figure 10, and the F1 score, recall and precision are presented in Table 4.

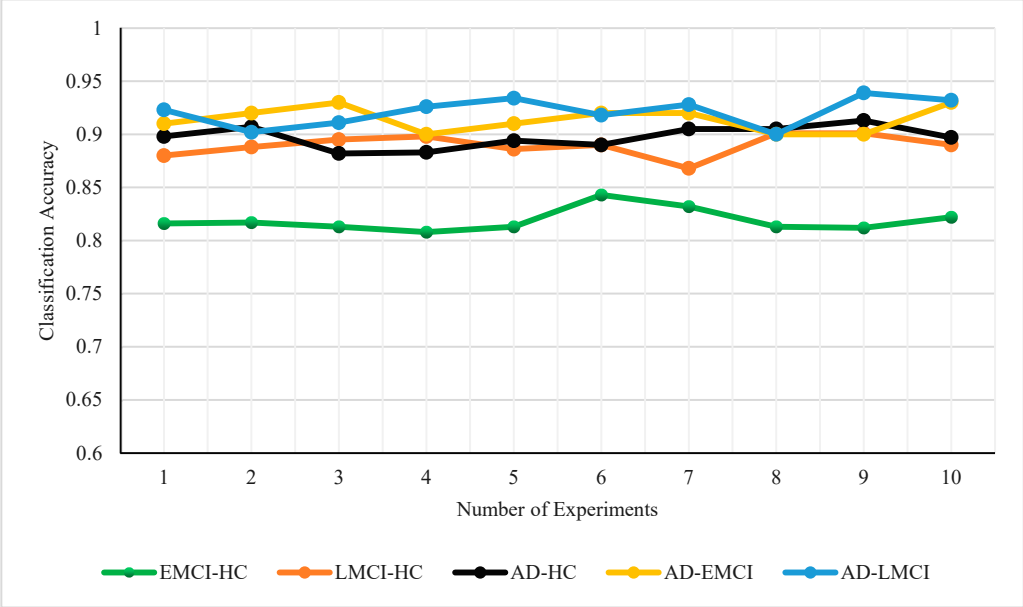

Figure 10. The 10 independent validation experiments accuracy of leave-one-out cross-validation of the test set in 5 datasets. HC = Healthy Control; EMCI = Early Mild Cognitive Impairment; LMCI = Late Mild Cognitive Impairment; AD = Alzheimer's Disease.

Table 4. The F1 score, recall and precision of the 10 independent validation experiments in test set. HC = Healthy Control; EMCI = Early Mild Cognitive Impairment; LMCI = Late Mild Cognitive Impairment; AD = Alzheimer's Disease.

Group	Accuracy	F1 Score	Recall	Precision
EMCI-HC	81.88% ± 1.02%	83.30% ± 0.78%	83.60% ± 0.80%	83.30% ± 0.78%
LMCI-HC	88.97% ± 0.97%	91.60% ± 0.80%	92.80% ± 0.87%	90.80% ± 0.60%
AD-HC	89.73% ± 0.98%	92.20% ± 0.75%	94.00% ± 0.63%	91.10% ± 0.83%
AD-EMCI	90.20% ± 1.54%	93.20% ± 1.08%	93.30% ± 1.19%	93.50% ± 1.02%
AD-LMCI	92.13% ± 1.27%	94.70% ± 1.00%	94.70% ± 1.00%	94.70% ± 1.00%

We observed that in the 10 independent experiments, our model achieved the highest accuracy of 93.9%. Moreover, across the five datasets, the difference in accuracy ranged from 3% to 3.9%. This indicates that our model demonstrates stable performance across different datasets.

4. Discussion

In this study, we proposed the multi-kernel SVM-Apriori model to mine the important features that performed well in classifying AD patients and healthy control. We compared our model with the traditional SVM and validated its stability on five different datasets. The results showed that the proposed multi-kernel SVM-Apriori model exhibited excellent classification performance and stability.

By leveraging the prior properties of frequent itemsets, the essence of the Apriori algorithm lies in discovering frequent itemsets through a layer-by-layer search. In this paper, we combine this algorithm with multi-kernel SVM, utilizing the advantages of multi-kernel SVM in binary classification performance with small sample datasets. We set the average classification accuracy at each stage as the minimum support threshold. Then, we scan the dataset to calculate the support of the next candidate itemset, which is defined as the SVM classification accuracy, and compare it with the minimum support threshold. Itemsets with support exceeding the threshold are considered as N + 1 item frequent itemsets. Finally, we obtain the accuracy of each set of frequent itemsets through leave-one-out validation.

To ensure the reliability of the computational results, we used the leave-one-out cross-validation method for accuracy calculations in our model, and we also applied the same method in the control group. By analyzing Figure 5, we found that our model's highest accuracy is in the AD-EMCI group, reaching 93%, while the highest accuracy in the control group for the AD-HC group is 90.4%. This may be because there is a significant difference between AD and EMCI, and the fusion of brain region and gene features further amplifies this difference, resulting in all models achieving good accuracy in the AD-EMCI group. In the 10 independent experiments, we observe that the highest accuracy is in AD-LMCI group, reaching 93.9%. The difference in the AD-EMCI group is 0.3, while the difference in the AD-LMCI group is 0.39, indicating that the results of the AD-EMCI group are more stable. The confusion matrices of the five datasets are shown in Figure 11. We also used the time series information to calculate the variance of each brain region in the AD-LMCI group, AD-EMCI group and AD-HC group. The variance of hippocampus, parahippocampal gyrus and amygdala in AD-EMCI group and AD-HC group are shown in Table 5. We found that in 90 brain regions, the AD-EMCI group exhibited higher variance in 64 brain regions compared to the AD-HC group. This indicates that the imaging data in these 64 brain regions have greater differences, which may contribute to the higher accuracy of the AD-EMCI group compared to the AD-HC group. Additionally, in the AD-HC and AD-LMCI groups, our model's accuracy also exceeded 90%, indicating significant differences in features between the AD group and the other three groups, which contributes to the excellent classification performance.

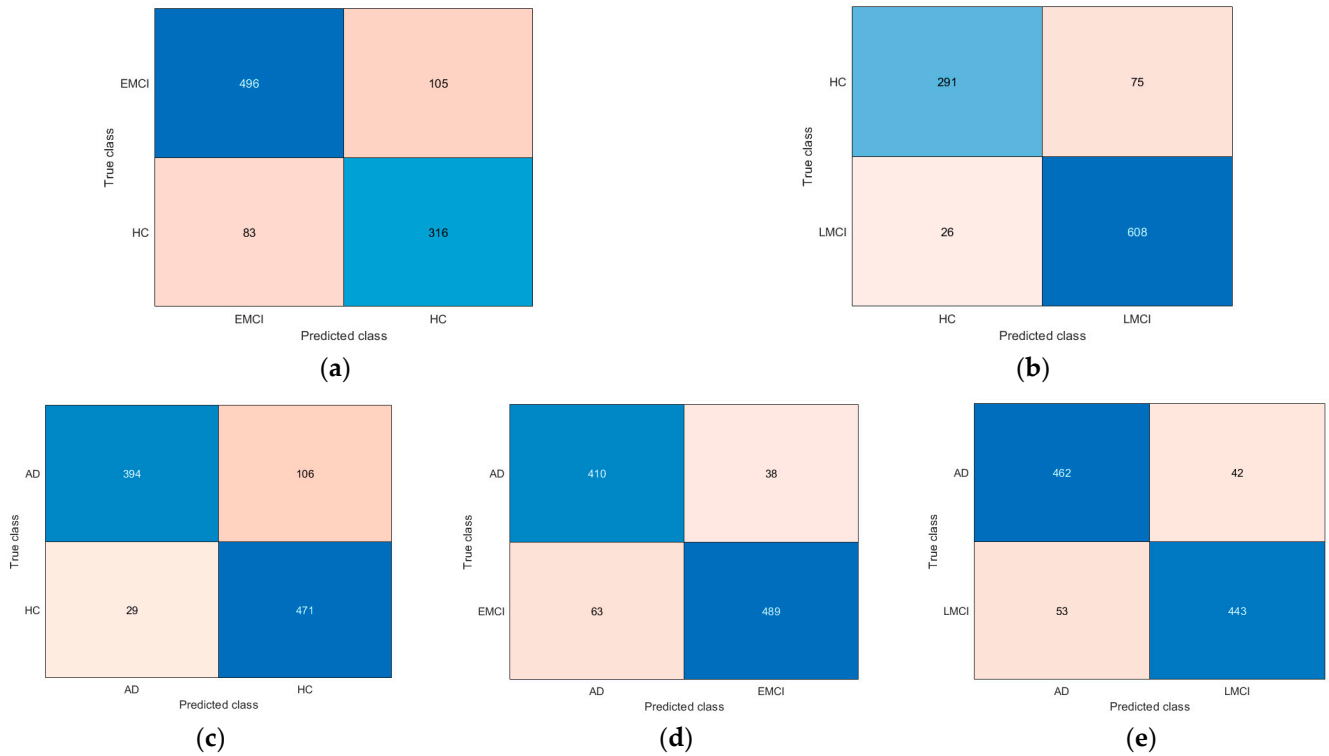

Figure 11. The confusion matrices of 5 datasets. (**a**) The confusion matrices of S_{EMCI_HC}. (**b**) The confusion matrices of S_{LMCI_HC}. (**c**) The confusion matrices of S_{AD_HC}. (**d**) The confusion matrices of S_{AD_EMCI}. (**e**) The confusion matrices of S_{AD_LMCI}. HC = Healthy Control; EMCI = Early Mild Cognitive Impairment; LMCI = Late Mild Cognitive Impairment; AD = Alzheimer's Disease.

Table 5. The variance of hippocampus, parahippocampal gyrus and amygdala in AD-EMCI group and AD-HC group. HC = Healthy Control; EMCI = Early Mild Cognitive Impairment; LMCI = Late Mild Cognitive Impairment; AD = Alzheimer's Disease.

Brain Region	AD-EMCI	AD-HC
Left hippocampus	0.178128395	0.001062739
Right hippocampus	0.13044139	0.055262965
Left parahippocampal gyrus	0.080443747	0.034482065
Right parahippocampal gyrus	0.045045533	0.008222377
Left amydala	0.11497812	0.044599828
Right amydala	0.089006046	0.117985895

In the EMCI-HC group, our model's accuracy reached 83.8%. Although lower than the accuracy of the other four groups, it still surpassed the control group's accuracy, with a maximum difference of 14.6%. This demonstrates that even though there are small differences in features between the EMCI and HC groups, the introduction of the Apriori algorithm helped select important features, leading to the SVM model with excellent classification performance when fused with the Apriori algorithm.

The brain region gene pairs that effectively classify AD and HC might represent potential pathogenic factors of AD. Our research detected some abnormal subregions and pathogenic genes associated with AD, such as the amygdala, *BIN1*, *RPN2* and *IL15*. We calculated the frequency of the identified genes and brain regions. Then, we selected the top genes and brain regions with a frequency above two to count their relation. The results are shown in Figure 12 (https://hiplot.com.cn/basic?lang=zh_cn, accessed on 29 April 2023).

Consistent with the results in Reference [27], the amygdala has been identified as an important brain region, and our proposed method achieved an accuracy of 93.9% after leave-one-out validation. The amygdala played an important role in AD [28–30]. Feng et al. [31] explored the microstructural changes in the amygdala of AD patients and identified the radiological characteristics of the amygdala as potential biomarkers for diagnosing AD. Hu et al. [32] performed GWAS using 1034 and 1186 participants and found multi SNPs at *BIN1* associated with AD. Other studies showed that the genotype patterns at *BIN1* were associated with memory performance [33] and identifying new SNPs at *BIN1* [34,35]. Suzuki et al. [36] investigated the cerebrovascular-specific molecular mechanisms of Alzheimer's disease (AD) and discovered that in the endothelial cells of the blood vessels in AD brain, there was an upregulation of protein (*RPN2*) associated with protein processing and N-glycosylation in the endoplasmic reticulum. This upregulation was correlated with the expression of ribosomal proteins. The *RPN1*, *RPN2*, *DDOST*, and *STT3A* formed the oligosaccharyltransferase complex, which was a membrane protein complex [37]. *RPN1* and *RPN2* could promote N-glycosylation [38,39]. This indicated that in the vascular endothelium of AD brains, the process of adding glycan chains to nascent polypeptides in the endoplasmic reticulum was enhanced [36]. Rentzos et al. [40] studied the effect of *IL15* and AD and found that the levels of *IL-15* in the cerebrospinal fluid of Alzheimer's disease are significantly elevated and show a significant positive correlation with the age of onset. Asby et al. [41] found *IL-15* was raised in AD patients and with systemic infection. Janelidze et al. [42] proved that *IL-15* was raised in CSF and associated with Aβ pathology. In our experiments, we also discovered *BIN1*, *RPN2*, and *IL15*, achieving excellent accuracy, F1 score, recall, and precision. This indicates that not only does our experiment perform well in AD classification, but it also demonstrates outstanding performance in detecting biomarkers related to AD.

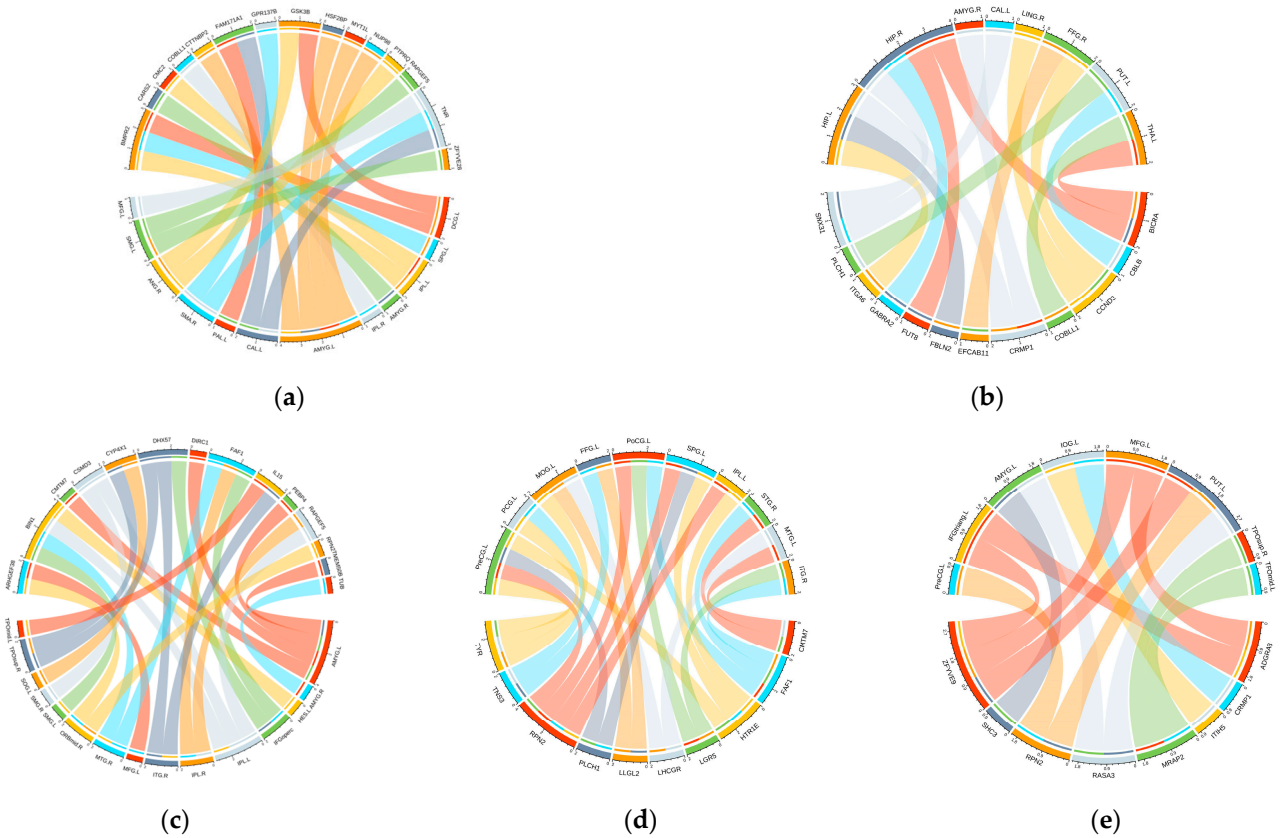

Figure 12. The relation of brain region gene pairs with their frequency above 2. (**a**) The relation of brain region and gene in EMCI-HC group; (**b**) The relation of brain region and gene in LMCI-HC group; (**c**) The relation of brain region and gene in AD-HC group; (**d**) The relation of brain region and gene in AD-EMCI group; (**e**) The relation of brain region and gene in AD- LMCI group. HC = Healthy Control; EMCI = Early Mild Cognitive Impairment; LMCI = Late Mild Cognitive Impairment; AD = Alzheimer's Disease.

5. Conclusions

In this study, we proposed a novel Multi-Kernel SVM–Apriori Model to extract the important features fusing information by brain regions and genes. Firstly, we conducted brain region and gene association analysis using the information from dual-gene chains. Our method effectively fused imaging and gene information, providing excellent candidate features for subsequent analysis. Additionally, we proposed the Multi Kernel SVM-Apriori Model to extract fusion features with significant contributions to AD classification. Finally, by combining feature fusion and the Multi-Kernel SVM–Apriori Model, we established an AD diagnostic framework and detected abnormal brain regions and pathogenic genes in AD, such as the amygdala, *BIN1*, *RPN2*, and *IL15*. However, our work also has some limitations. Our study may benefit from utilizing more diverse datasets encompassing various demographics, disease stages, and ethnicities. Expanding the dataset could enhance the generalizability and robustness of our proposed model. Although our method effectively fused imaging and gene information, future studies could explore more advanced feature selection techniques to identify the most informative and discriminative features for AD classification, opening up new research directions for the diagnosis and treatment of AD.

Author Contributions: Z.H., X.M., B.H. and W.L. led and supervised the research. Z.H., X.M., B.H. and W.L. designed the research and wrote the article. Z.H., C.T., S.C. and S.X. performed the data processing, visualization of results. C.T., Y.L. and X.N. performed data pre-processing and quality control. Z.H., X.M. and W.L. revised the manuscript. All authors have read and agreed to the published version of the manuscript.

Funding: This study was funded by the National Natural Science Foundation of China (6237010008), the MOE (Ministry of Education in China) Project of Humanities and Social Sciences (19YJCZH120), the Science and Technology Plan Project of Changzhou (CZ20230028, CJ20220151) and the Natural Science Foundation of the Jiangsu Higher Education Institutions of China (23KJB520002). This work was also sponsored by the Qing Lan Project of Jiangsu Province (2020).

Data Availability Statement: The studies involving Q10 human participants were reviewed and approved by Data collection and sharing for this project was funded by the Alzheimer's Disease Neuroimaging Initiative (ADNI). We applied the access from ADNI. The patients/participants provided their written informed consent to participate in this study. Written informed consent was obtained from the individual(s) for the publication of any potentially identifiable images or data included in this article.

Acknowledgments: Data collection and sharing for this project was funded by the Alzheimer's Disease Neuroimaging Initiative (ADNI). The complete ADNI Acknowledgement is available at http://adni.loni.usc.edu/wp-content/uploads/how_to_apply/ADNI_Acknowledgement_List.pdf (accessed on 15 May 2020).

Conflicts of Interest: The authors declare no conflicts of interest.

References

1. Association, A.S. 2019 Alzheimer's disease facts and figures. *Alzheimer's Dement.* **2019**, *15*, 321–387. [CrossRef]
2. Jiao, Z.; Ji, Y.; Jiao, T.; Wang, S. Extracting Sub-Networks from Brain Functional Network Using Graph Regularized Nonnegative Matrix Factorization. *Comput. Model. Eng. Sci.* **2020**, *123*, 845–871. [CrossRef]
3. Agosta, F.; Galantucci, S.; Filippi, M. Advanced magnetic resonance imaging of neurodegenerative diseases. *Neurol. Sci.* **2017**, *38*, 41–51. [CrossRef]
4. Moradi, E.; Pepe, A.; Gaser, C.; Huttunen, H.; Tohka, J. Machine learning framework for early MRI-based Alzheimer's conversion prediction in MCI subjects. *NeuroImage* **2015**, *104*, 398–412. [CrossRef]
5. Huang, Y.; Su, Y.; Byun, Y.; Lee, Y.; Kim, S. Analysis of multiple chronic disease characteristics in middle-aged and elderly South Koreans by exercise habits based on association rules mining algorithm. *BMC Public Health* **2023**, *23*, 1232. [CrossRef]
6. Vougas, K.; Sakellaropoulos, T.; Kotsinas, A.; Foukas, G.-R.P.; Ntargaras, A.; Koinis, F.; Polyzos, A.; Myrianthopoulos, V.; Zhou, H.; Narang, S.; et al. Machine learning and data mining frameworks for predicting drug response in cancer: An overview and a novel in silico screening process based on association rule mining. *Pharmacol. Ther.* **2019**, *203*, 107395. [CrossRef]
7. Liu, Y.; Wang, L.; Miao, R.; Ren, H. A Data Mining Algorithm for Association Rules with Chronic Disease Constraints. *Comput. Intell. Neurosci.* **2022**, *2022*, 8526256. [CrossRef] [PubMed]
8. Hadavi, S.M.S.; Oliaei, S.; Saidi, S.; Nadimi, E.; Kazemi-Galougahi, M.H. Using Data Mining and Association Rules for Early Diagnosis of Esophageal Cancer. *Gulf J. Oncol.* **2022**, *1*, 38–46.
9. Zhang, D.; Wang, Y.; Zhou, L.; Yuan, H.; Shen, D. Multimodal classification of Alzheimer's disease and mild cognitive impairment. *NeuroImage* **2011**, *55*, 856–867. [CrossRef] [PubMed]
10. An, L.; Adeli, E.; Liu, M.; Zhang, J.; Shen, D. Semi-supervised Hierarchical Multimodal Feature and Sample Selection for Alzheimer's Disease Diagnosis. In Proceedings of the Medical Image Computing and Computer-Assisted Intervention—MICCAI 2016, Athens, Greece, 17–21 October 2016; pp. 79–87.
11. Wu, A.T.H.; Lawal, B.; Wei, L.; Wen, Y.-T.; Tzeng, D.T.W.; Lo, W.-C. Multiomics Identification of Potential Targets for Alzheimer Disease and Antrocin as a Therapeutic Candidate. *Pharmaceutics* **2021**, *13*, 1555. [CrossRef] [PubMed]
12. Lai, Y.; Lin, X.; Lin, C.; Lin, X.; Chen, Z.; Zhang, L. Identification of endoplasmic reticulum stress-associated genes and subtypes for prediction of Alzheimer's disease based on interpretable machine learning. *Front. Pharmacol.* **2022**, *13*, 975774. [CrossRef] [PubMed]
13. Tian, Y.; Lu, Y.; Cao, Y.; Dang, C.; Wang, N.; Tian, K.; Luo, Q.; Guo, E.; Luo, S.; Wang, L.; et al. Identification of diagnostic signatures associated with immune infiltration in Alzheimer's disease by integrating bioinformatic analysis and machine-learning strategies. *Front. Aging Neurosci.* **2022**, *14*, 919614. [CrossRef] [PubMed]
14. Yang, B.; Bao, W.; Hong, S. Alzheimer-Compound Identification Based on Data Fusion and forgeNet_SVM. *Front. Aging Neurosci.* **2022**, *14*, 931729. [CrossRef] [PubMed]
15. Zhang, F.; Petersen, M.; Johnson, L.; Hall, J.; O'Bryant, S.E. Recursive Support Vector Machine Biomarker Selection for Alzheimer's Disease. *J. Alzheimer's Dis.* **2021**, *79*, 1691–1700. [CrossRef] [PubMed]
16. Olatunji, S.O.; Alansari, A.; Alkhorasani, H.; Alsubaii, M.; Sakloua, R.; Alzahrani, R.; Alsaleem, Y.; Alassaf, R.; Farooqui, M.; Basheer Ahmed, M.I.; et al. Preemptive Diagnosis of Alzheimer's Disease in the Eastern Province of Saudi Arabia Using Computational Intelligence Techniques. *Comput. Intell. Neurosci.* **2022**, *2022*, 5476714. [CrossRef] [PubMed]
17. Jiao, Z.; Chen, S.; Shi, H.; Xu, J. Multi-Modal Feature Selection with Feature Correlation and Feature Structure Fusion for MCI and AD Classification. *Brain Sci.* **2022**, *12*, 80. [CrossRef] [PubMed]

18. Syaifullah, A.H.; Shiino, A.; Kitahara, H.; Ito, R.; Ishida, M.; Tanigaki, K. Machine Learning for Diagnosis of AD and Prediction of MCI Progression From Brain MRI Using Brain Anatomical Analysis Using Diffeomorphic Deformation. *Front. Neurol.* **2021**, *11*, 576029. [CrossRef]
19. Houria, L.; Belkhamsa, N.; Cherfa, A.; Cherfa, Y. Multi-modality MRI for Alzheimer's disease detection using deep learning. *Phys. Eng. Sci. Med.* **2022**, *45*, 1043–1053. [CrossRef]
20. Yan, C.-G.; Wang, X.-D.; Zuo, X.-N.; Zang, Y.-F. DPABI: Data Processing & Analysis for (Resting-State) Brain Imaging. *Neuroinformatics* **2016**, *14*, 339–351. [CrossRef]
21. Jenkinson, M.; Beckmann, C.F.; Behrens, T.E.; Woolrich, M.W.; Smith, S.M.J.N. Fsl. *Neuroimage* **2012**, *62*, 782–790. [CrossRef]
22. Tzourio-Mazoyer, N.; Landeau, B.; Papathanassiou, D.; Crivello, F.; Etard, O.; Delcroix, N.; Mazoyer, B.; Joliot, M. Automated Anatomical Labeling of Activations in SPM Using a Macroscopic Anatomical Parcellation of the MNI MRI Single-Subject Brain. *NeuroImage* **2002**, *15*, 273–289. [CrossRef]
23. Saykin, A.J.; Shen, L.; Foroud, T.M.; Potkin, S.G.; Swaminathan, S.; Kim, S.; Risacher, S.L.; Nho, K.; Huentelman, M.J.; Craig, D.W.; et al. Alzheimer's Disease Neuroimaging Initiative biomarkers as quantitative phenotypes: Genetics core aims, progress, and plans. *Alzheimer's Dement.* **2010**, *6*, 265–273. [CrossRef]
24. Purcell, S.; Neale, B.; Todd-Brown, K.; Thomas, L.; Ferreira, M.A.R.; Bender, D.; Maller, J.; Sklar, P.; de Bakker, P.I.W.; Daly, M.J.; et al. PLINK: A Tool Set for Whole-Genome Association and Population-Based Linkage Analyses. *Am. J. Hum. Genet.* **2007**, *81*, 559–575. [CrossRef]
25. Zhang, X.; Xie, Y.; Tang, J.; Qin, W.; Liu, F.; Ding, H.; Ji, Y.; Yang, B.; Zhang, P.; Li, W.; et al. Dissect Relationships Between Gene Co-expression and Functional Connectivity in Human Brain. *Front. Neurosci.* **2021**, *15*, 797849. [CrossRef]
26. Jeong, B.; Lee, J.; Kim, H.; Gwak, S.; Kim, Y.K.; Yoo, S.Y.; Lee, D.; Choi, J.-S. Multiple-Kernel Support Vector Machine for Predicting Internet Gaming Disorder Using Multimodal Fusion of PET, EEG, and Clinical Features. *Front. Neurosci.* **2022**, *16*, 856510. [CrossRef] [PubMed]
27. Meng, X.; Wu, Y.; Liu, W.; Wang, Y.; Xu, Z.; Jiao, Z. Research on Voxel-Based Features Detection and Analysis of Alzheimer's Disease Using Random Survey Support Vector Machine. *Front. Neuroinform.* **2022**, *16*, 856295. [CrossRef] [PubMed]
28. Murray, A.N.; Chandler, H.L.; Lancaster, T.M. Multimodal hippocampal and amygdala subfield volumetry in polygenic risk for Alzheimer's disease. *Neurobiol. Aging* **2021**, *98*, 33–41. [CrossRef] [PubMed]
29. An, N.; Fu, Y.; Shi, J.; Guo, H.-N.; Yang, Z.-W.; Li, Y.-C.; Li, S.; Wang, Y.; Yao, Z.-J.; Hu, B.; et al. Synergistic Effects of APOE and CLU May Increase the Risk of Alzheimer's Disease: Acceleration of Atrophy in the Volumes and Shapes of the Hippocampus and Amygdala. *J. Alzheimer's Dis.* **2021**, *80*, 1311–1327. [CrossRef]
30. Caesar, M.H.; Nateka, L.J.; Abbi, R.H.; Lori, L.M. Impairments in Fear Extinction Memory and Basolateral Amygdala Plasticity in the TgF344-AD Rat Model of Alzheimer's Disease Are Distinct from Nonpathological Aging. *eNeuro* **2022**, *9*, ENEURO.0181-0122.2022. [CrossRef]
31. Feng, Q.; Niu, J.; Wang, L.; Pang, P.; Wang, M.; Liao, Z.; Song, Q.; Jiang, H.; Ding, Z. Comprehensive classification models based on amygdala radiomic features for Alzheimer's disease and mild cognitive impairment. *Brain Imaging Behav.* **2021**, *15*, 2377–2386. [CrossRef]
32. Hu, X.; Pickering, E.; Liu, Y.C.; Hall, S.; Fournier, H.; Katz, E.; Dechairo, B.; John, S.; Van Eerdewegh, P.; Soares, H.; et al. Meta-Analysis for Genome-Wide Association Study Identifies Multiple Variants at the BIN1 Locus Associated with Late-Onset Alzheimer's Disease. *PLoS ONE* **2011**, *6*, e16616. [CrossRef]
33. Barral, S.; Bird, T.; Goate, A.; Farlow, M.R.; Diaz-Arrastia, R.; Bennett, D.A.; Graff-Radford, N.; Boeve, B.F.; Sweet, R.A.; Stern, Y.; et al. Genotype patterns at *PICALM*, *CR1*, *BIN1*, *CLU*, and *APOE* genes are associated with episodic memory. *Neurology* **2012**, *78*, 1464. [CrossRef] [PubMed]
34. Carrasquillo, M.M.; Belbin, O.; Hunter, T.A.; Ma, L.; Bisceglio, G.D.; Zou, F.; Crook, J.E.; Pankratz, V.S.; Sando, S.B.; Aasly, J.O.; et al. Replication of BIN1 Association with Alzheimer's Disease and Evaluation of Genetic Interactions. *J. Alzheimer's Dis.* **2011**, *24*, 751–758. [CrossRef] [PubMed]
35. Lee, J.H.; Cheng, R.; Barral, S.; Reitz, C.; Medrano, M.; Lantigua, R.; Jiménez-Velazquez, I.Z.; Rogaeva, E.; St. George-Hyslop, P.H.; Mayeux, R. Identification of Novel Loci for Alzheimer Disease and Replication of CLU, PICALM, and BIN1 in Caribbean Hispanic Individuals. *Arch. Neurol.* **2011**, *68*, 320–328. [CrossRef] [PubMed]
36. Suzuki, M.; Tezuka, K.; Handa, T.; Sato, R.; Takeuchi, H.; Takao, M.; Tano, M.; Uchida, Y. Upregulation of ribosome complexes at the blood-brain barrier in Alzheimer's disease patients. *J. Cereb. Blood Flow Metab.* **2022**, *42*, 2134–2150. [CrossRef]
37. Kelleher, D.J.; Gilmore, R. An evolving view of the eukaryotic oligosaccharyltransferase. *Glycobiology* **2005**, *16*, 47R–62R. [CrossRef]
38. Honma, K.; Iwao-Koizumi, K.; Takeshita, F.; Yamamoto, Y.; Yoshida, T.; Nishio, K.; Nagahara, S.; Kato, K.; Ochiya, T. RPN2 gene confers docetaxel resistance in breast cancer. *Nat. Med.* **2008**, *14*, 939–948. [CrossRef]
39. Wilson, C.M.; High, S. Ribophorin I acts as a substrate-specific facilitator of N-glycosylation. *J. Cell Sci.* **2007**, *120*, 648–657. [CrossRef]
40. Rentzos, M.; Zoga, M.; Paraskevas, G.P.; Kapaki, E.; Rombos, A.; Nikolaou, C.; Tsoutsou, A.; Vassilopoulos, D. IL-15 Is Elevated in Cerebrospinal Fluid of Patients With Alzheimer's Disease and Frontotemporal Dementia. *J. Geriatr. Psychiatry Neurol.* **2006**, *19*, 114–117. [CrossRef]

41. Asby, D.; Boche, D.; Allan, S.; Love, S.; Miners, J.S. Systemic infection exacerbates cerebrovascular dysfunction in Alzheimer's disease. *Brain* **2021**, *144*, 1869–1883. [CrossRef]
42. Shorena, J.; Niklas, M.; Erik, S.; Olof, L.; Sebastian, P.; Henrik, Z.; Kaj, B.; Oskar, H. CSF biomarkers of neuroinflammation and cerebrovascular dysfunction in early Alzheimer disease. *Neurology* **2018**, *91*, e867. [CrossRef]